Creep behavior of an SiC-reinforced XD™ $MoSi_2$ composite

M. Suzuki and S. R. Nutt
Brown University, Division of Engineering, Providence, RI 02912 (USA)
R. M. Aikin, Jr.
Case Western Reserve University, Department of Materials Science and Engineering, Cleveland, OH 44106 (USA)

Abstract

The compressive creep behavior of an $MoSi_2$–SiC composite and a base alloy was investigated at 1050–1300 °C. Creep experiments performed in air showed power-law type constitutive behavior with a stress exponent of approximately 3.5. Both materials showed some effect of thermal oxidation during creep. Microstructural observations by transmission electron microscopy indicated that deformation occurred primarily by dislocation glide and that the rate-controlling process was recovery by dislocation climb. In the composite material, SiC particles were effective impediments to glide, as were numerous strain centers, tentatively identified as coherent precipitate particles. Cavitation occurred at SiC–matrix interfaces and at grain boundaries within polycrystalline SiC particles, and the process was apparently facilitated by the accumulation of glassy phase at these sites during creep. High resolution electron microscopy observations indicated the glassy phase originated both from thermal oxidation during creep and from non-crystalline material that pre-existed in the as-fabricated composite.

1. Introduction

There is a growing need for structural materials capable of service above 1200 °C in oxidizing atmospheres, particularly for applications such as gas turbine engines and spacecraft airframes. However, present state-of-the-art materials such as nickel-based superalloys, limit aerospace designers to maximum service temperatures of about 1100 °C. $MoSi_2$ is one candidate material that may satisfy the needs described above. $MoSi_2$ has a high melting point (2030 °C) and is currently used for heating elements at temperatures as high as 1900 °C [1]. It reportedly exhibits good oxidation resistance, which arises from the formation of a protective SiO_2 film [2].

Like most intermetallic compounds, there are major problems preventing the use of $MoSi_2$ in structural applications. The problems for $MoSi_2$ include low ductility and poor impact strength at lower temperatures (less than 1000 °C), and relatively low strength at higher temperatures (above 1000 °C). This behavior is related to the relatively low brittle–ductile transition temperature (approximately 1000 °C) [3]. (There is some disagreement as to the value of the transition temperature, and some investigators have observed the brittle-to-ductile transition to lie between 1300 and 1400 °C [4]. It is likely that the brittle-to-ductile transition temperature is a function of grain size and impurity content.) In order to develop $MoSi_2$ as a viable high-temperature structural material, these properties must be improved.

Several attempts have been made to fabricate $MoSi_2$-based composites with the goal of improving strength and creep resistance at high temperatures, and enhancing fracture toughness and ductility at room temperature. Petrovic *et al.* showed that the addition of SiC whiskers improved the fracture toughness and flexural strength of $MoSi_2$ and attributed this to crack deflection and dispersion strengthening by the SiC whiskers [5–8]. Further improvement in fracture toughness was realized by adding ZrO_2 particles, which led to microcracking in $MoSi_2$ induced by the ZrO_2 transformation, as well as high dislocation densities [9]. In other work, Lu *et al.* demonstrated toughness enhancement in $MoSi_2$ through the addition of niobium particles, which tended to rupture in a ductile fashion [10]. Alloying $MoSi_2$ with other C11b disilicides such as WSi_2 has also been shown to improve high-temperature mechanical properties, although at the cost of increased density [8].

Although the investigations described above relied on powder metallurgical (PM) processing routes, $MoSi_2$-based composites can also be synthesized by *in situ* processes. Henager and Brimhall synthesized $MoSi_2$/Sic composites using a solid state displacement reaction between Mo_2C and Si [11], while Aikin synthesized $MoSi_2$-based composites with TiB_2, ZrB_2, HfB_2 and SiC using an *in situ* synthesis process

0921-5093/93/$6.00

(XD™), developed at Martin Marietta Laboratories [12]. Both studies demonstrated improvements in mechanical properties of $MoSi_2$. One advantage of *in situ* processing is that it is possible to introduce a wide range of thermodynamically stable reinforcements and control the particle morphology. In addition, *in situ* processes generally produce microstructures with substantially less glass phase than silicides produced by conventional powder processing. Powder processing of $MoSi_2$ typically produces undesirable amounts of SiO_2 glass phase that originates from oxide films on the starting powder surfaces [13]. Furthermore, in one investigation of PM processed $MoSi_2$–SiC_w composites, the whiskers were chemically attacked by impurities present in the source powders used for the matrix [5, 14]. The *in situ* processes referenced above are expected to produce cleaner interfaces between SiC and $MoSi_2$ than conventional powder processing, thus avoiding such deleterious effects.

To date, there have been relatively few studies of the relation between creep properties and microstructure of $MoSi_2$ and $MoSi_2$ composites [15, 16]. Understanding creep properties, including the mechanisms of deformation and damage that limit component lifetime and cause failure, is of critical importance to the development of such materials for high-temperature structural use. Sadananda *et al.* reported the compressive creep behavior of monolithic $MoSi_2$ and 20% SiC whisker-reinforced $MoSi_2$ at 1100–1400 °C in air [15]. They measured a stress exponent of 3 for both materials, and apparent activation energies of 590 kJ mol^{-1} and 430 kJ mol^{-1} for the composite and the monolithic $MoSi_2$ respectively. The addition of SiC whiskers reduced the compressive creep rate by nearly 2 orders of magnitude. In other work, Umakoshi *et al.* reported the compressive creep behavior of $MoSi_2$ single crystals at 1200–1400 °C [16]. They measured a stress exponent of 3, and an apparent activation energy of 520 kJ mol^{-1}.

Although studies of the creep behavior of $MoSi_2$ and $MoSi_2$ composites are few, microstructural observations of crept samples are fewer. Careful examination of crept microstructures is necessary to determine mechanisms of deformation and damage in composites, because unlike monolithic materials, such mechanisms cannot be reliably inferred from measured stress exponents [17]. The objective of the present study is to determine the mechanisms of creep deformation and damage in $MoSi_2$–SiC composites. The approach involves measurements of compressive creep response of a base alloy ($MoSi_2$) and an $MoSi_2$–SiC composite in an aerobic test atmosphere (air), followed by direct observations of crept microstructures by transmission electron microscopy (TEM) and correlation with the measured response.

2. Experimental procedure

Two materials were included in this study: a composite reinforced with 30 v/o SiC, fabricated *in situ* by the XD™ process, and a base alloy of polycrystalline $MoSi_2$, fabricated by consolidating a commercially available $MoSi_2$ powder. The $MoSi_2$ composite was produced at Martin Marietta Laboratories, and although aspects of the XD™ process are considered proprietary, the basis is as follows. First, an $MoSi_2$ composite sponge was produced by XD™ synthesis, and the sponge was then crushed to produce at -50 mesh $MoSi_2$–SiC composite powder. A fully dense $MoSi_2$ composite was produced by hot-pressing the -50 mesh $MoSi_2$ composite powder at 1800 °C and 20 MPa for 4 h in a graphite die, followed by hot isostatic pressing at 1600 °C and 310 mPa for 2 h. $MoSi_2$ composites fabricated by this method reportedly exhibit oxidation resistance similar to $MoSi_2$ [18]. The base alloy was produced by hot-pressing a -325 mesh $MoSi_2$ powder (Consolidated Astronautics, a division of CERAC) at 1800 °C and 20 MPa for 4 h in a graphite die, followed by hot isostatic pressing at 1800 °C and 207 MPa for 4 h. Table 1 shows the chemical compositions of the composite and the base alloy [12]. Note the higher content of oxygen, nitrogen and carbon in the base alloy.

Cylindrical specimens 3 mm × 6 mm in length were cut by EDM and end polished for creep experiments. Compressive creep experiments were conducted at 1050–1300 °C under applied stresses of 35–300 MPa. The experiments were conducted under constant load in continuously circulated air. The displacement of the upper SiC platen was monitored with a linear variable-differential transducer, and a plot of strain rate *vs.* time

TABLE 1. Chemical composition of the composite and the base alloy [12]

Material	[Mo]/[Si] ratio		Interstitial elements			Reinforcements (vol.%)
	Mo(at.%)	Si(at.%)	O(wt.%)	N(wt.%)	C(wt.%)	
Composite	33.4	66.6	0.13	0.018	n.a.	29.1
Base alloy	32.2	67.8	0.65	0.100	0.376	—

was used to determine that a constant creep rate (or minimum strain rate) was reached and maintained [19]. The stress (or temperature) was then changed incrementally, and the procedure was repeated. The test temperature was maintained to within ±1 °C of the preset value, and specimens were held at the test temperature for at least 30 min before the load was applied. Upon completion of a test, specimens were cooled rapidly under stress to retain the deformed microstructure. The strain in each specimen was kept under 3% to minimize non-uniform deformation (barreling).

Thin foil specimens were prepared for TEM observation by sectioning a disk from the center of each cylindrical specimen. The discs were ground and polished and finally thinned by Ar ion-milling. The thin foils were examined using a Philips EM420T operated at 120 kV and equipped with a double-tilt specimen holder and an energy dispersive X-ray (EDS) spectrometer. High resolution electron microscopy (HREM) experiments were carried out using a JEOL 2010 operated at 200 kV. The 2010 was equipped with a parallel detection electron energy loss spectrometer (PEELS, made by GATAN). The $MoSi_2$ composite and the base alloy were examined in pretest and crept conditions to determine changes associated with creep.

3. Results

3.1. Fabricated microstructure

A variety of precipitate phases was present within the composite and the base alloy. Optical micrographs of both materials are shown in Fig. 1. The SiC reinforcements in the composite appear as gray equiaxed particles, 1–15 μm in size, and the distribution is slightly non-uniform. A prominent second phase, later identified as CMo_5Si_3 [19], appears as white particles adjacent to the SiC and these are 1–10 μm in diameter. The average grain size of the composite is approximately 10 μm, almost half the grain size in the base alloy (approximately 20 μm). The grain refinement was attributed to the presence of SiC particles, which pinned migrating grain boundaries during hot-pressing, and the fact that composite hot-pressing was done at a slightly lower temperature.

The base alloy contained an unexpected number of inclusion particles, as shown in Fig. 1(b), a metallographic section revealing the typical microstructure. The majority of the second-phase particles exhibit gray contrast, and these were later identified as β-SiC by TEM examination. Although not expected, this observation can be explained by carbon present in the source powders (see Table 1). The darker particles

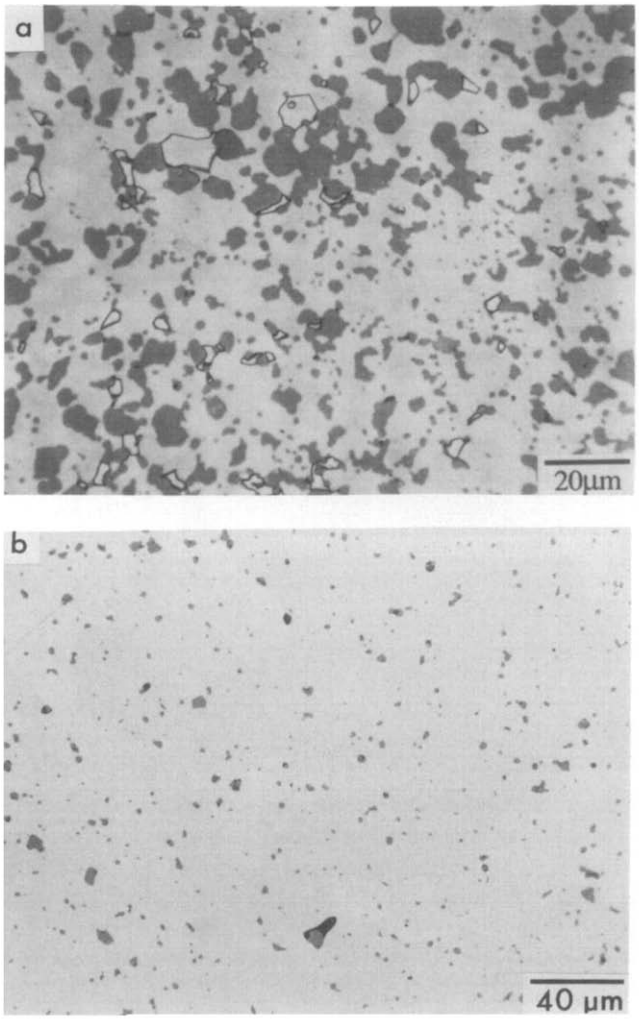

Fig. 1. Metallography of (a) the $MoSi_2$ composite and (b) the base alloy after etching with a modified Murakami's reagent (15 g $K_3Fe(CN_6)$, 2 g NaOH, 100 ml water).

were identified as SiO_2 glass and these were more abundant than in the composite. The observation of more abundant oxide phase in the base alloy is consistent with the high oxygen content in the base alloy mentioned previously (Table 1).

TEM examination of the composite revealed single-crystal and polycrystalline β-SiC particles at grain boundaries (Fig. 2(a)). The particles typically contained defects, including twins, stacking faults, dislocations, and occasionally small (approximately 0.2 nm) inclusions also. Small amounts of glass phase were sometimes observed within particles. A typical region, shown in Fig. 2(a), depicts a faceted SiC particle with some small adjacent inclusion phases. These inclusions were identified as CMo_5Si_3, SiO_2 glass, and occasionally $MoSi_2$ (C11b, not shown), and $MoSi_2$ (C40, a phase stabilized by impurities, also not shown) [19]. The morphology and proximity of the CMo_5Si_3 phase,

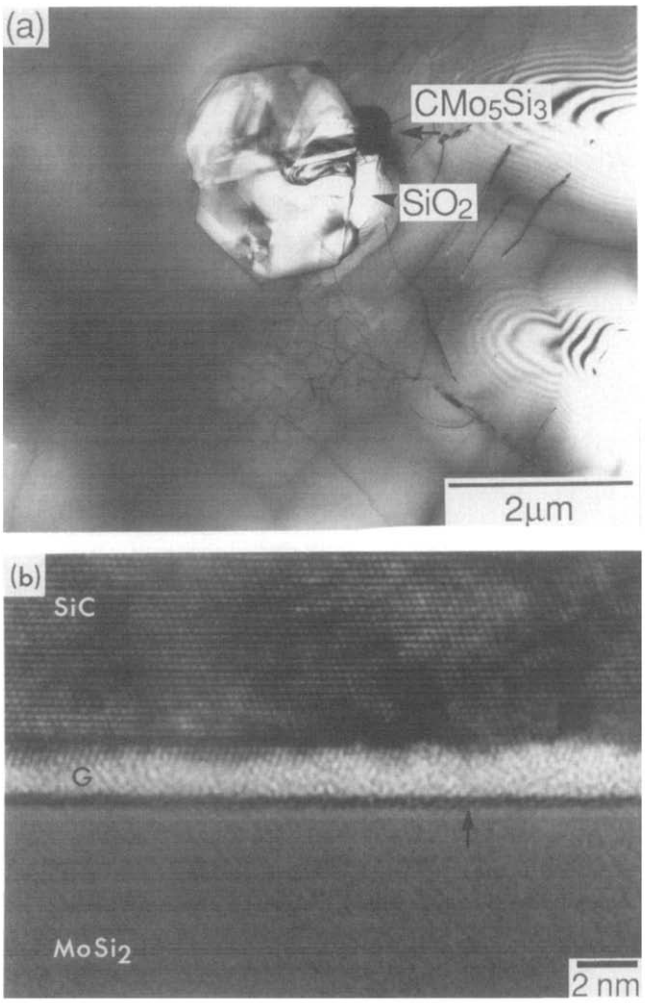

Fig. 2. Microstructural features in as-fabricated materials: (a) TEM bright-field image of β-SiC particle and network of sub-boundary dislocations; (b) interfacial glass film (G) separating β-SiC particle and the silicide matrix, the arrow indicates a possible molybdenum-rich layer.

which was always adjacent to the SiC particles, suggested that CMo_5Si_3 resulted from fluctuations in local composition associated with the formation of the SiC particles. Similar morphologies were observed in a carbon-modified $MoSi_2$ in which SiC phase formed *in situ* during fabrication [20, 21].

Diffraction-contrast imaging techniques, including bright-field and diffuse-scatter dark-field imaging, failed to reveal any glassy phase at triple grain junctions or at grain boundary–interface (GBI) junctions in the composite. ("Grain boundary–interface junction" refers to a triple junction formed where a matrix grain boundary intersects a matrix–particle interface). However, phase-contrast (HREM) images revealed thin (0.5–1.5 nm) glassy films at GBI junctions and at grain boundaries within polycrystalline β-SiC particles, as shown in Fig. 2(b). The image also shows a thin line of dark contrast separating the glass phase and the silicide matrix, apparently a consequence of Fresnel diffraction. No consistent crystallographic orientation relationships were detected between the matrix and the β-SiC particles, or between grains within the polycrystalline β-SiC particles.

The base alloy showed some of the same inclusion phases adjacent to SiC particles, such as CMo_5Si_3 and silica glass. However, compositional analysis by EDS of the CMo_5Si_3 in the base alloy indicated that the phase contained substantial amounts of impurities, including Ti and Fe [19]. The concentration levels of the impurities imply that the atoms substitute into the structure with relative ease. These particles were rarer in the base alloy (and much smaller) than in the composite owing to the much lower SiC volume fraction. Unlike most PM silicides produced by hot-pressing, glass phase was not detected at triple grain junctions.

3.2. Creep behavior

Isothermal creep behavior for the composite was determined by plotting strain rate *vs.* time for stress levels that were increased incrementally. Minimum strain rates were achieved for a range of stress levels at 1050–1300 °C, and these are plotted as a function of applied stress in Fig. 3. The plots show data obtained from experiments in air for applied stress levels ranging from 35 to 300 MPa. The data conform to a power-law constitutive relation ($\sigma \propto \dot{\varepsilon}^n$) with a stress exponent of approximately 3.5. The response is similar to results reported by others, as cited in Section 1 [15, 16]. A stress exponent of 3 often implies a dislocation creep mechanism [22, 23], although more rigorous documentation is generally required to determine creep deformation mechanisms in composite materials.

The apparent activation energies for creep were obtained from an Arrhenius plot of creep rates *vs.* inverse temperature for a fixed stress. The data obtained at 1100 °C–1300 °C yielded an apparent activation energy of 430 kJ mol^{-1}, slightly lower than values reported elsewhere for similar materials [15]. Because the activation energy is single valued over the temperature range 1100–1300 °C, the rate-controlling process is assumed to be unchanged for this regime. The process(es) associated with the measured values of activation energies can be determined by careful examination of the crept microstructure, described later.

Creep tests conducted on the base alloy at 1200 °C showed behavior similar to the composite. Figure 3(b) shows creep data for the base alloy for stress levels of 42–130 MPa. Creep data for the composite at 1200 °C are included for comparison. The data conform to a power-law constitutive relation with a stress exponent of approximately 3, just as for the composite material, and in accordance with reports of creep behavior of

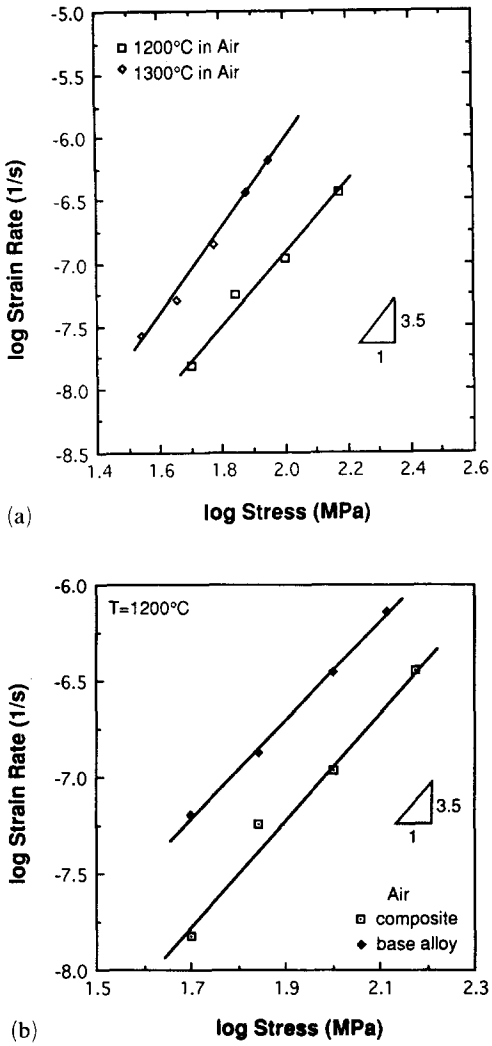

Fig. 3. Steady-state (minimum) strain rates *vs.* applied stress (a) for the composite and (b) for the base alloy in circulated air (composite data shown for comparison).

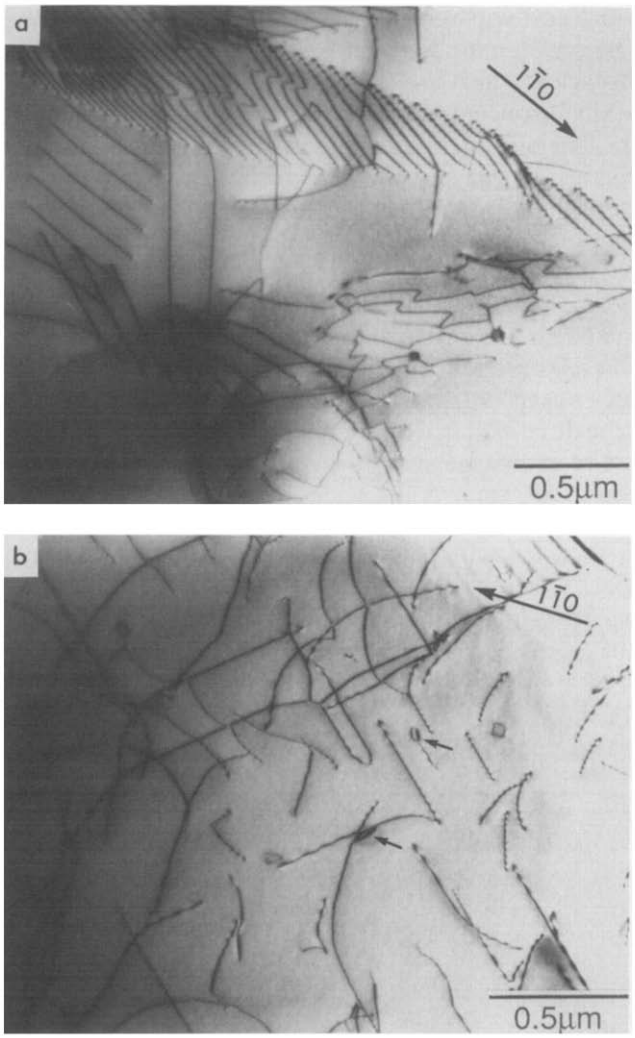

Fig. 4. Dislocation substructure in the composite after creep at 1300 °C: (a) typical sub-boundary configuration; (b) loop configurations indicated by arrows result from pinning by small precipitates.

similar materials [15, 16]. In monolithic ceramics, a stress exponent of around 3 is normally associated with creep deformation by dislocation glide [22, 23]. As expected, the creep rate of the base alloy was higher than that of the composite, but only by a factor of about 3.5.

3.3. Microstructure after creep

TEM observations of composite specimens deformed at 1050–1300 °C revealed an increase in the density of matrix dislocations. After creep at 1100 °C, matrix dislocations were distributed uniformly and there was a slight tendency to form networks. However, after creep at 1300 °C, the tendency to form networks and subgrain boundaries was more pronounced, resulting in configurations such as shown in Fig. 4(a). The dislocation segments tended to be straight unless intersected by other defects, where they often showed zigzag configurations. Analysis of the defects revealed that the intragranular glide dislocations had Burgers vectors of the type ⟨100⟩, while network dislocations in subboundaries had Burgers vectors of the type ⟨100⟩, ⟨110⟩ and $\frac{1}{2}$⟨111⟩, an indication of energetically favorable reactions during recovery [19]. Similar observations were reported for $MoSi_2$ deformed in compression [24, 25].

A salient feature of the deformed microstructures was the high density of matrix dislocations around reinforcement particles [12, 19]. Glide during creep was impeded by SiC particles, producing dense tangles and pileups, particularly between particles in close proximity. Several smaller inclusions are also apparent in the image, and these appear to obstruct glide also. Further evidence of impeded glide was evidenced by the numerous dislocation loops that appeared, some of

which are apparent in Fig. 4(b), indicated by arrows. The configurations result from dislocations pinned by obstacles, which are surrounded by loops that appear as small concentric rings [26]. The loop configurations are generally intersected by straight segments of dislocation also, suggesting that they form by Orowan bowing rather than by vacancy condenstaion. In several cases, multiple concentric loops were observed around a strain center, indicating that Orowan bowing occurred more than once, as previously pinned dislocations passed the strain centers and left loops behind. The obstacles are tentatively identified as coherent precipitates based on analysis of diffraction contrast images, to be described in a future publication.

Creep damage at 1050–1300 °C occurred by cavitation at SiC–matrix interfaces and at grain boundaries within polycrystalline SiC particles. Figure 5(a) shows cavitation at a grain boundary–interface junction (GBI) that occurred during creep at 1200 °C. Glassy phase was typically present around the peripheral regions of cavities, and the process of cavitation was apparently facilitated by accumulation of glass phase during creep. Figure 5(b) shows an energy loss spectrum from the glass pocket, revealing the presence of silicon, oxygen, and a small amount of molybdenum. Accumulations of glass phase were attributed to redistribution of thin interfacial films present in the pretested composite and to partial dissolution and oxidation of the silicide matrix. Redistribution of glass films during creep deformation can reportedly lead to cavitation at sites of stress concentration such as GBI junctions [17].

An important aspect of the creep process was the concurrent thermal oxidation that occurred at the surface of the specimen. Figure 6(a) shows a metallographic section of the near-surface region after creep at 1200 °C. The cross-section shows a surface oxide layer (presumably a silicate glass) about 2–3 μm thick, as well as evidence of oxide penetration along grain boundaries (arrow). The dark particles are SiC. The

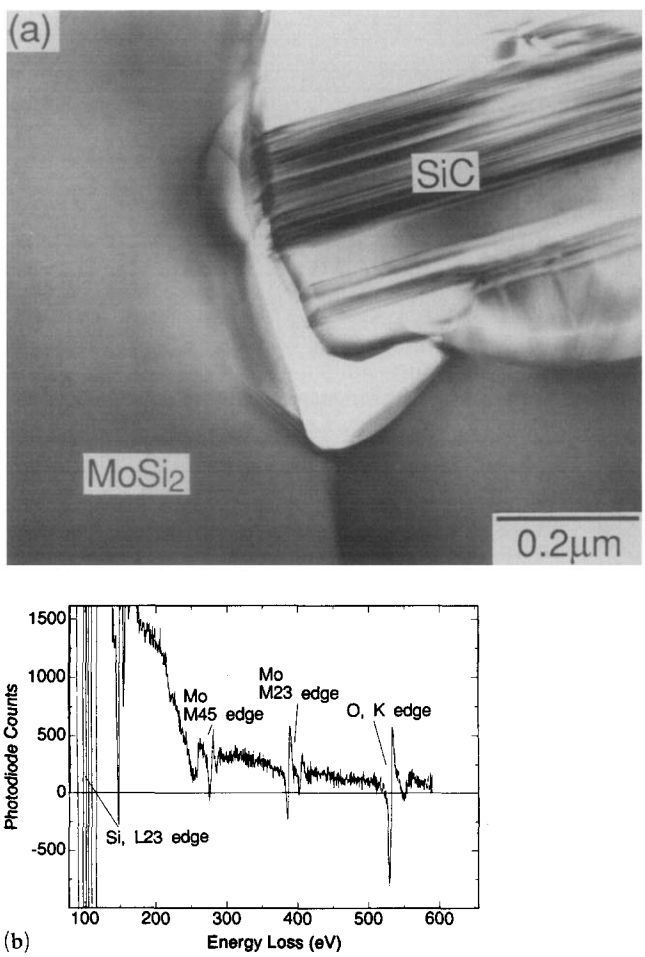

Fig. 5. Creep damage by cavitation in composite at 1200 °C: (a) cavity at GBI junction lined with glass film; (b) PEELS spectrum of glass accumulation at composite interface, showing silicon, oxygen, and a small amount of molybdenum.

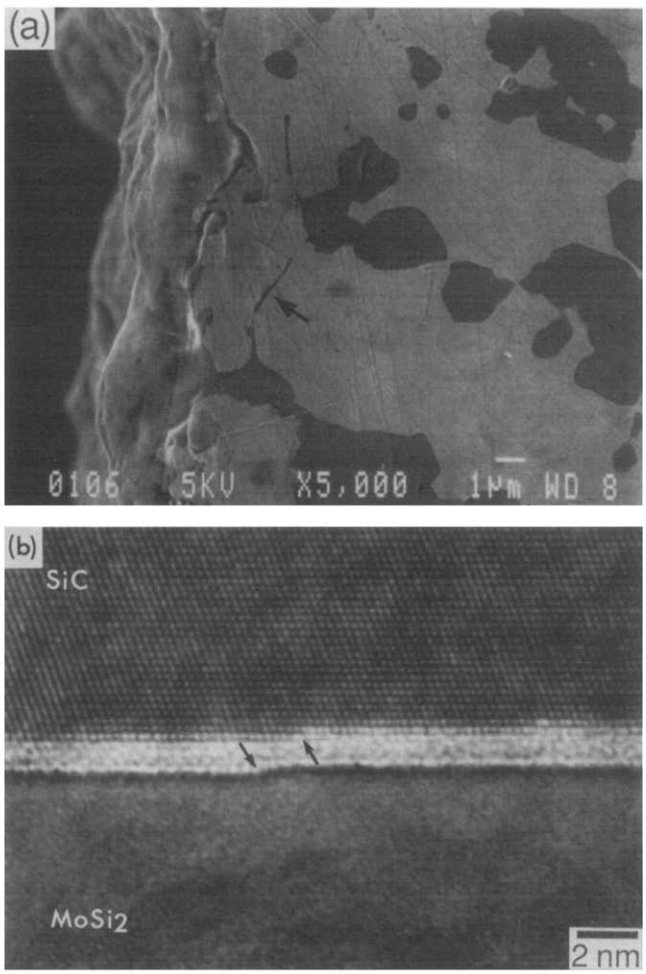

Fig. 6. Composite oxidation during creep in air at 1200 °C: (a) polished section showing oxide scale and penetration of oxide films along grain boundaries (arrow); (b) interfacial oxide glass film similar to pretested microstructure.

formation of a protective surface layer of silica is not unexpected, and is in fact responsible for the inherent oxidation resistance of $MoSi_2$ [27]. However, the penetration of oxide into the composite during creep is another matter with potentially deleterious consequences. Figure 6(b) shows a phase-contrast image of the interface beween the matrix and a β-SiC particle after creep at 1200 °C. Compositional analysis of the glassy film indicated that the film contained predominantly silicon and oxygen with a small amount of molybdenum. Both boundaries are flat and parallel, and it is interesting to note that even the monatomic ledge on the SiC facet is replicated by the silicide matrix. Either the matrix and particle were at one time in contact and later became separated by an influx of glass phase, or a chemical reaction occurred to produce the film, the thickness of which is strictly controlled by thermodynamic factors governing equilibrium [28]. In addition, the image shows dark-line contrast between the glass film and silicide matrix that was noted previously in Fig. 2. The dark-line contrast was invariant with defocus, and the behavior was attributed to the presence of a molybdenum-rich film resulting from the dissolution of a small amount of $MoSi_2$ at the interface. Assuming oxidation is occurring to a limited extent at such interfaces during creep, it is possible that some of the silicide dissolves in the glassy film, leaving a molybdenum-rich layer. It is likely that further oxidation would produce MoO_3, an oxide that reportedly forms concurrently with SiO_2 when $MoSi_2$ is oxidized [27]. Thin films of glassy silica were also present at grain boundaries within polycrystalline β-SiC particles. The implication of these observations is that oxidation appears to occur at interfaces and grain boundaries during creep in aerobic test ambients, albeit to a limited extent, and that glassy films are generally present at interfaces during creep.

To test the effect of stress on oxidation behavior, a similar specimen was annealed in air at 1200 °C for the same time as the creep test. Scanning electron microscopy (SEM) observations of near-surface regions showed an oxidation layer of similar thickness, but relatively more uniform, and the penetration of oxide along grain boundaries was less frequent. HREM observations showed that the thickness of the glass films present at internal boundaries tended to be less than in the crept specimen. These observations imply that oxidation (and oxide penetration) into the sample was facilitated by the compressive stress.

Creep deformation of the base alloy produced microstructural changes similar to those noted in the composite. The density of matrix dislocations was substantially increased, and the density was generally higher around inclusions and near subgrain boundaries. Subgrain boundaries, which were also present prior to creep deformation, apparently served as sources and sinks for dislocations during creep. There was little evidence of creep damage in the base alloy, even at likely nucleation sites such as SiC or SiO_2 particles, matrix interfaces, or grain boundary junctions. Cavitation did not occur despite substantial creep strains (the total strain in the base alloy was about 2.7%). The absence of cavitation is somewhat surprising given that the base alloy appeared to contain more glass phase than the composite prior to creep. It is well established that glass phase facilities cavitation and grain boundary sliding during creep, and thus more glass phase should translate into faster creep and greater creep damage. However, the absence of cavitation does appear to be consistent with the smaller volume fraction of hard particles, which often provide nucleation sites for cavitation during creep deformation.

Microstructural effects of thermal oxidation during creep were more apparent in the base alloy than in the composite. The number and size of second-phase particles in the base alloy was substantially increased compared with the pretest microstructure (*cf.* Fig. 1(b)). Moreover, many of the particles exhibited dark contrast associated with the SiO_2 phase, as discussed in Section 3.1, indicating that thermal oxidation occurred during creep. This is attributed to the higher dissolved oxygen content in the base alloy, noted in Table 1. TEM observations of the same specimens showed that the additional second-phase particles were predominantly multiphase agglomerates of glass particles that contained impurity-bearing phases [21]. These particles were unlike those in the as-fabricated material, indicating that the impurity content of the base alloy had a deleterious effect on the oxidation behavior.

SEM examination of near-surface regions revealed additional evidence of increased thermal oxidation and penetration of reaction product into the material. In addition to the formation of an oxide skin as in the composite material, the base alloy showed more extensive penetration of oxide along grain boundaries. The oxide was continuous along grain boundaries near the outer surface of the cylindrical creep specimen, and discontinuous at greater distances inward.

4. Discussion

4.1. Creep deformation mechanisms

Based on the measured stress exponent (approximately 3.5) and the observed increase in the density of matrix dislocations after creep, it was concluded that creep deformation in the composite occurred primarily by dislocation motion [22, 23]. The test temperatures were above the reported brittle–ductile transition for

$MoSi_2$, and it is likely that dislocations were relatively mobile under these conditions. SiC reinforcement particles were effective barriers to dislocation glide, impeding glide and causing tangles and pileups of dislocations in the vicinity of particles. The increased resistance to creep observed in the composite was thus attributed primarily to the obstruction of dislocation motion by the hard reinforcing particles. Differences in dislocation substructure after creep at 1100 °C and 1300 °C (Section 3.3) were attributed to an increased rate of dynamic recovery by dislocation climb at the higher temperature. These observations imply that dislocation climb was the rate-controlling process for creep deformation.

The measured apparent activation enerty (430 kJ mol^{-1}), corresponds to thermally activated processes that were dominant under these conditions. Unfortunately, data are not presently available for the activation energies for lattice or grain boundary diffusion in $MoSi_2$. Creep by grain boundary sliding (assisted by viscous flow of intergranular glass) was probably a minor factor, because extensive dislocation activity was apparent and glassy phase was rarely detected at matrix grain boundaries. For example, Fig. 7(a) is a phase-contrast image of a matrix grain boundary after creep in air at 1200 °C, showing no intergranular glassy phase. The boundary happens to be atomically flat and constitutes a special high-symmetry boundary in which there is a high degree of coincidence. The grain orientations are [111] and [110], and the boundary plane is $(\bar{1}10)$. Such boundaries were in fact exceptional, and are probably less suceptible to damage, although glass phase was generally not detected in significant quantities at any of the boundaries. A second example of a grain boundary glass film observed after creep at 1200 °C in air is shown in Fig. 7(b). The phase-contrast image shows a thin (less than 0.5 nm) amorphous film that is difficult to resolve because of a slight inclination of the boundary. Glass films at interfaces were far more common than intergranular films, and it is possible that some accommodation occurred by interfacial sliding during creep. However, the evidence supporting dislocation motion is overwhelming in all cases, and the component of creep strain associated with boundary sliding is probably small.

A creep damage mechanism of apparently secondary importance was cavitation at interfaces and grain boundaries in SiC particles. The process of cavitation was facilitated by the accumulation of the glass phase during creep (Fig. 5(a)). Probable sources of the glass phase include glass films present in the pretested composite (Fig. 2(b)), and silica glass produced by thermal oxidation of $MoSi_2$ and SiC during creep (Figs. 6 and 7(b)). The relative contributions from these sources are uncertain, and parallel creep experiments in non-oxidizing atmospheres are needed.

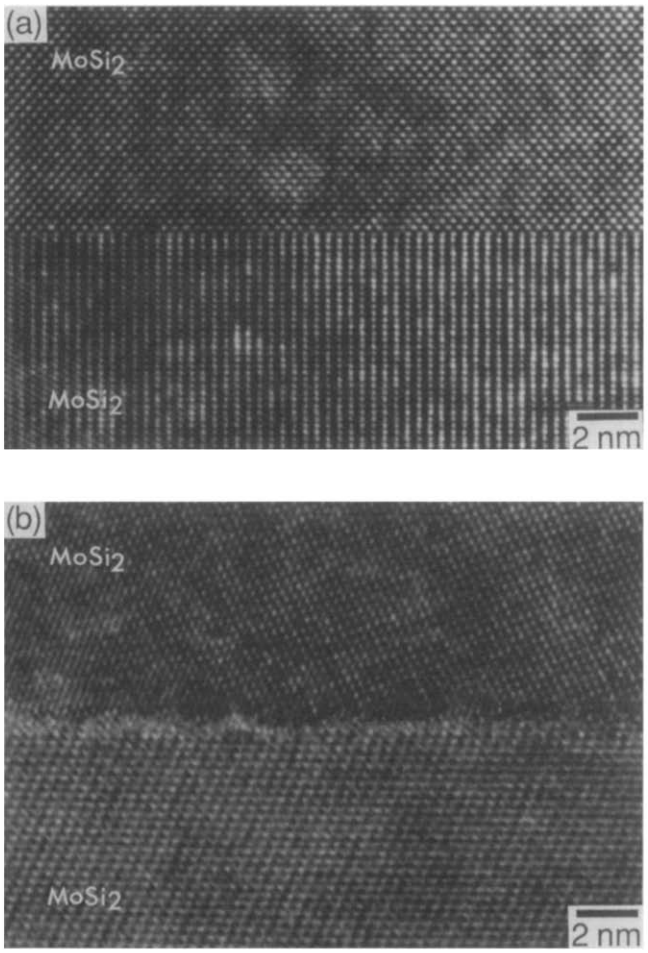

Fig. 7. Grain boundary structure in composite and base alloy after creep in air at 1200 °C: (a) glass-free grain boundary in composite matrix; (b) grain boundary in base alloy showing trace of glass film.

4.2. Strain rates of the composite and the base alloy

The difference of strain rate between the composite and the base alloy at 1200 °C was a factor of approximately 3.5 (Fig. 3). The strain rate differences were surprisingly small, considering the higher glass phase content of the base alloy, the negligible creep damage, and the 50 times difference reported elsewhere for similar materials [15]. The reason for the similar strain rates appears to lie primarily with the fact that the creep rate for the base alloy was low. This can be explained by the high levels of impurity originally present in the base alloy, which resulted in dispersion- and composite-strengthening and effectively lowered the creep rate. Although the average grain size in the base alloy was approximately twice that of the composite ($d = 20$ μm and $d = 10$ μm in the base alloy and composite respectively), the grain size should have little effect on the strain rate when creep deformation occurs by a dislocation mechanism [22].

Figure 8 shows a comparison of strain rates of the composite measured in this study with the strain rates

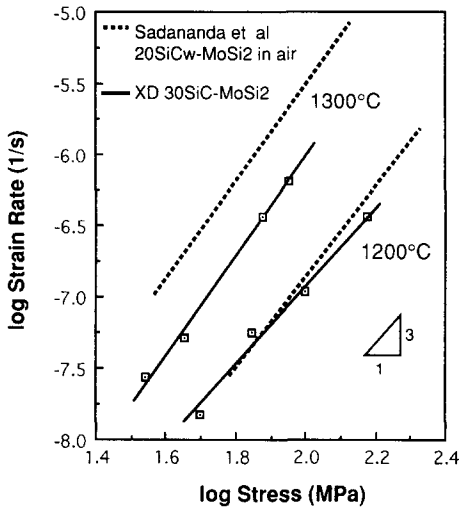

Fig. 8. Comparison of creep data in current study with data reported in ref. 15.

of a 20% SiC whisker-reinforced $MoSi_2$ at 1200 °C and 1300 °C [15]. The strain rates of the two composite materials at 1200 °C are similar, despite the difference in reinforcement volume fraction (20% whiskers *vs.* 30% particles). However, at 1300 °C, the strain rate of the whisker-reinforced $MoSi_2$ is greater than that of the particulate-reinforced composite in this study by a factor of about 3. At 1200 °C, the whisker geometry provides some fiber strengthening and may result in constraint hardening at fiber–fiber contacts, thus providing equivalent creep resistance with a lower volume fraction (20% *vs.* 30%). However, at 1300 °C, the whisker composite creeps more rapidly than the *in situ* composite. The PM processing undoubtedly causes higher levels of impurity concentration and associated intergranular glass phase, and SiC whiskers reportedly react with certain impurities, possibly causing property degradation [5, 14]. The difference in strain rates indicates a possible advantage to *in situ* processing compared with powder blending routes for $MoSi_2$ composites.

The reported strain rates for the base alloy in ref. 15 are apparently larger than those of the base alloy in this study by factors of more than 10. Furthermore, the stress dependence of the strain rate appears to be about 1.5. These differences are related to the different microstructures of the two alloys, which includes glassy films along grain boundaries [15]. These differences, in turn, are likely to be related to differences in the purity of the starting materials, as well as differences in consolidation parameters. The grain boundary glass films should facilitate grain boundary sliding during creep, and the grain boundary sliding should cause accelerated strain rates and a lower stress exponent (approximately 1.5), as reported in ref. 15. In this study, the grain-boundary glass phase was thin (less than 0.5 nm) and possibly discontinuous (Fig. 7(b)), and the effect on grain boundary sliding was consequently small, as discussed in Section 4.1.

4.3. Atmospheric effects

The atmospheric effects on creep response of the composite were associated with thermal oxidation processes that occurred during the experiment. These processes, including the oxidation of $MoSi_2$ and SiC, resulted in slight thickening of glass-phase films along interfaces and with SiC particles. The only other observable effect on the microstructure was the higher frequency of oxide penetration along near-surface grain boundaries. Although it appeared to have only a minor effect on the creep behavior, this penetration appeared to be enhanced by the applied stress. The passivating layer formed on the composite during high-temperature creep apparently inhibits most of the deleterious effects of thermal oxidation. Whether this would be the case under tensile or flexural loading is uncertain.

The atmospheric effects on creep tended to be more pronounced in the base alloy than in the composite. The microstructural changes in the base alloy consisted of coarsened SiO_2 particles and formation of an oxide scale, phenomena which were attributed to both internal and surface oxidation. From this, one might conclude that the addition of SiC reinforcements actually enhances the oxidation resistance of $MoSi_2$. SiC, like $MoSi_2$, forms a surfacelayer of SiO_2 glass when oxidized, and under certain conditions, this layer protects from further oxidation. However, the issue is complicated by the higher impurity levels present in the base alloy, which may contribute to accelerated oxidation behavior, and it is consequently impossible to draw firm conclusions from the present data about the cause of the different oxidation behaviors. It is clear, though, that the increased presence of oxide glass particles and intergranular glass films was primarily responsible for the accelerated creep rates observed in air.

5. Summary and conclusions

Compressive creep experiments on SiC-reinforced XD™ $MoSi_2$ and a base alloy at 1050–1300 °C in air yielded the following results.

(1) The creep deformation mechanism of the composite involved dislocation glide in which the rate-controlling process was dislocation climb. Some creep damage occurred by cavitation at SiC–matrix interfaces and at grain boundaries within polycrystalline SiC particles. This process was apparently facilitated by the

accumulation of glassy phase at these sites during creep.

(2) The creep deformation mechanism in the base alloy was also dislocation motion, but cavitation in the base alloy was rarely observed.

(3) SiC particles and coherent precipitates hardened the composite matrix by impeding the motion of dislocations and grain boundaries.

(4) *In situ* processed composites may have advantages over powder-blended composites for high-temperature applications involving oxidizing environments.

Acknowledgments

The research was supported by the Office of Naval Research contract N00014-91-J-1480 (MS and SRN), and by DARPA through NADC contract N62269-89-C-0233 (RA). Financial support from UBE Industries, Ltd. (MS) is also gratefully acknowledged.

References

1 J. Schlichting, *High Temp. High Pressures, 10* (1978) 241–269.
2 P. J. Meschter, *Scripta Metall., 25* (1991) 1065–1069.
3 E. Fitzer, O. Rubisch, J. Schlichting and I. Sewdas, *Sci. Ceram., 6* (1973) XVIII.
4 R. M. Aikin, Jr., *Scripta Metall., 26* (1992) 1025–1030.
5 F. D. Gac and J. J. Petrovic, *J. Am. Ceram. Soc., 68* (8) (1985) C-200–C-201.
6 W. S. Gibbs, J. J. Petrovic and R. E. Honnel, *Ceram. Eng. Sci. Proc., 8* (7–8) (1987) 645–648.
7 D. H. Carter, J. J. Petrovic, R. E. Honnel and W. S. Gibbs, *Ceram. Eng. Sci. Proc., 10* (9–10) (1989) 1121–1129.
8 J. J. Petrovic and R. E. Honnel, *Ceram. Eng. Sci. Proc., 11* (7–8) (1990) 734–744.
9 J. J. Petrovic, R. E. Honnel and T. E. Mitchell, *Ceram. Eng. Sci. Proc., 12* (9–10) (1991) 1633–1642.
10 T. C. Lu, A. G. Evans, R. J. Hecht and R. Mehrabian, *Acta. Metall., 39* (1991) 1853–1862.
11 C. H. Henager, Jr., and J. L. Brimhall, *Scripta Metall., 26* (1992) 585–589.
12 R. M. Aikin, *Mater. Sci. Eng., A155* (1992) 121–133.
13 J. D. Cotton, Y. S. Kim and M. J. Kaufman, *Mater. Sci. Eng., A144* (1991) 287–291.
14 J.-M. Yang and S. M. Jeng, *J. Mater. Res., 6* (1991) 505–513.
15 K. Sadananda, H. Jones, J. Feng, J. J. Petrovic and A. K. Vasudevan, *Ceram. Eng. Sci. Proc., 12* (9–10) (1991) 1671–1678.
16 Y. Umakoshi, *Bull. Jpn. Inst. Metals, 30* (1991) 72–79.
17 P. Lipetzky, S. R. Nutt, D. A. Koester and R. F. Davis, *J. Am. Ceram. Soc., 74* (6) (1991) 1240–1247.
18 J. Cook, R. Mahapatra, E. W. Lee, A. Khan and J. Waldman, *Ceram. Eng. Sci. Proc., 12* (9–10) (1991) 1656–1670.
19 S. Suzuki, *MS Thesis*, Brown University, Providence, RI, 1992.
20 S. Jayashankar and M. J. Kaufman, *Scripta Metall., 26* (1992) 1245–1250.
21 S. Maloy, A. H. Heuer, J. J. Lewandowski and J. J. Petrovic, *J. Am. Ceram. Soc., 74* (10) (1991) 2704–2706.
22 J. Cadek, *Creep in Metallic Materials*, Elsevier, Amsterdam, 1988.
23 W. R. Cannon and T. G. Langdon, *J. Mater. Sci., 18* (1983) 1–28.
24 Y. Umakoshi, T. Sakagami, T. Hirano and T. Yamane, *Acta Metall., 38* (1990) 909–915.
25 O. Unal, J. J. Petrovic, P. H. Carter and T. E. Mitchell, *J. Am. Ceram. Soc., 73* (6) (1990) 1752–1757.
26 J. Edington, *Practical Electron Microscopy in Materials Science*, Philips, Eindhoven, 1974, 144–154.
27 C. G. McKamey, P. F. Tortorelli, J. H. DeVan and C. A. Carmichael, *J. Mater. Res., 7* (10) (1992) 2747–2755.
28 D. R. Clarke, *J. Am. Ceram. Soc., 70* (1) (1987) 15–22.